Three-Dimensional Solution-Adaptive Grid Generation on Composite Configurations

Yen Tu*
Air Force Armament Laboratory, Eglin Air Force Base, Florida 32542
and
Joe F. Thompson†
Mississippi State University, Mississippi State, Mississippi 34762

Abstract

THE EAGLE 3D composite-block grid code has been coupled with an implicit Euler flow solver to generate solution-adaptive grids for composite-block configurations with an improved control function formulation. The code has been tested with two complex composite configurations, one of which, an eight-block finned body of revolution at transonic speeds, is described here. The solution-adaptive grids obtained are shown to possess continuous slopes across block boundaries and an improved quality of aerodynamics simulation about complex geometries.

Contents

The ideal of solution-adaptive grid generations is to sense some gradients in the evolving physical solutions and have the grid points cluster in the regions of high gradients in the solution as they emerge so that the accuracy of flow solutions can be improved. Furthermore, the approach to construct composite-block grids with complete continuity across boundaries between blocks appears very flexible and useful in treating complex configurations (cf. Refs. 1-3).

The technique used is based on the following elliptic grid generation equation and a definition of control function[1-3]

$$\sum_{i=1}^{3}\sum_{j=1}^{3} g^{ij} r_{\xi^i\xi^j} + \sum_{k=1}^{3} g^{kk} P_k r_{\xi^k} = 0 \tag{1}$$

where

$$P_i = \sum_{j=1}^{3} \frac{g^{ij}}{g^{ii}} \frac{(W_i)_{\xi^j}}{W_i} \qquad (i = 1, 2, 3) \tag{2}$$

$$W = 1 + |\underline{\nabla} p| \tag{3}$$

where r is the position vector, g^{ij} the contravariant metric tensor, ξ^i the curvilinear coordinate, P_k the control function, W the weight function, and $\underline{\nabla} p$ the pressure gradient.

An eight-block finned body of revolution at an angle of attack of 12 deg with a Mach number of 0.95 and a 30-block ogive-cylinder-ogive multiple-store configuration at an angle of attack of 0 deg with a Mach number of 0.95 were tested.[3] Only the former case will be discussed here.

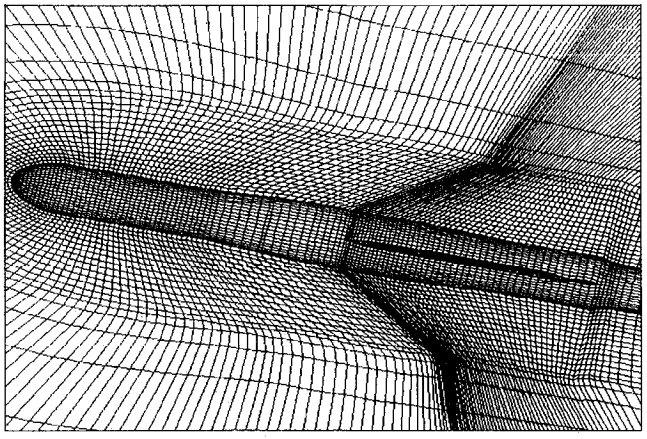

Fig. 1 Initial grid of finned body of revolution.

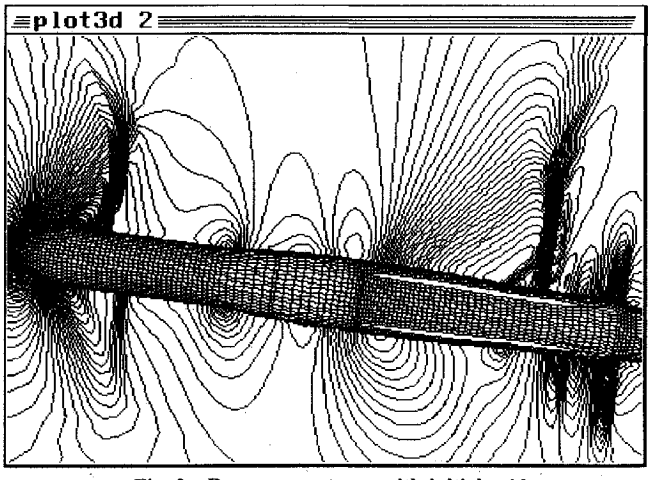

Fig. 2 Pressure contours with initial grid.

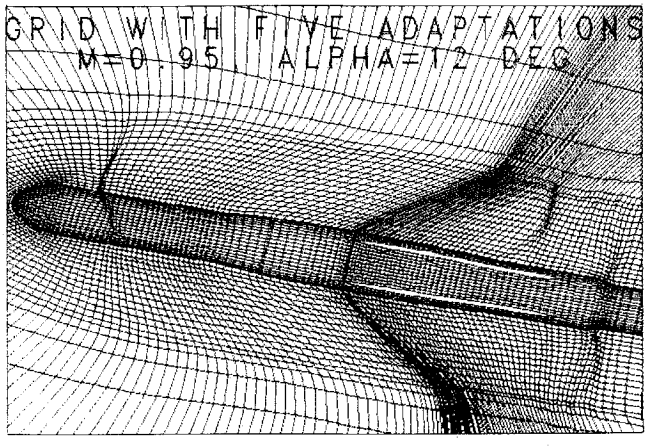

Fig. 3 Adaptive grid.

Presented as Paper 90-0329 at the AIAA 28th Aerospace Sciences Meeting, Reno, NV, Jan. 8-11, 1990; received Jan. 29, 1990; synoptic received Oct. 19, 1990; accepted for publication Oct. 19, 1990. Full paper available from AIAA Library, 555 W. 57th Street, New York, NY 10019, Price: microfiche, $4.00; hard copy, $9.00. **Remittance must accompany order.** This paper is declared a work of the U.S. Government and is not subject to copyright protection in the United States.

*Research Scientist, Computational Fluid Dynamics Section, Aerodynamics Branch, Aeromechanics Division. Member AIAA.
†Professor, Aerospace Department. Member AIAA.

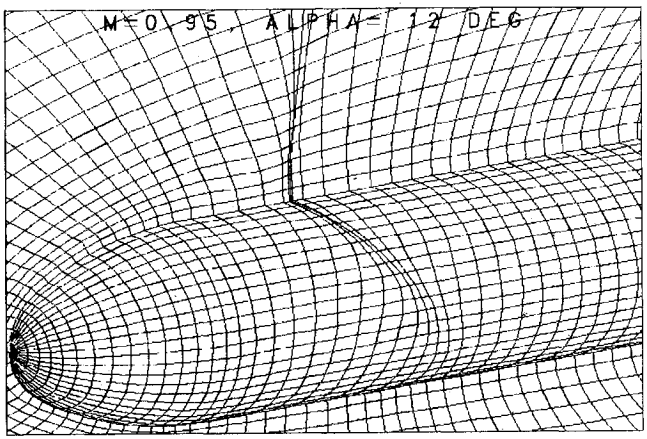

Fig. 4 Adaptive grid—nose section.

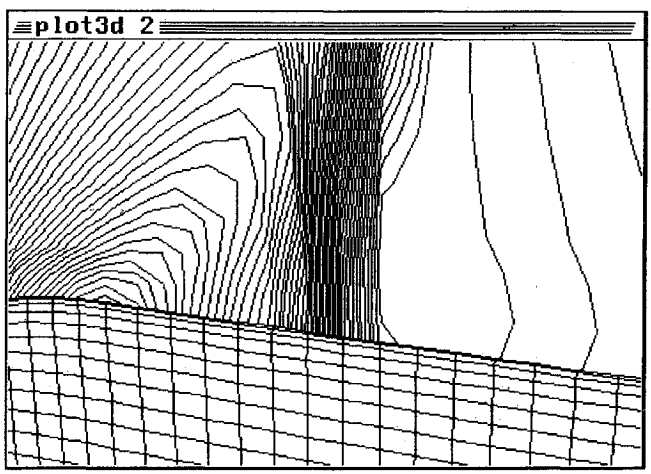

Fig. 5 Shock with initial grid.

Results

The grid of the finned body of revolution consists of eight blocks. Figure 1 shows the initial grid on the body and normal to the body surface. Figure 2 shows the pressure contours after 1000 cycles of solution calculations with the initial grid. Here, the fin grids were removed for clarity. It is observed that a strong shock occurs on the leeward side of the nose section and its strength decreases in the circumferential direction toward the windward side. There are shocks at the middle of the upper tail section and around the base of the body as well.

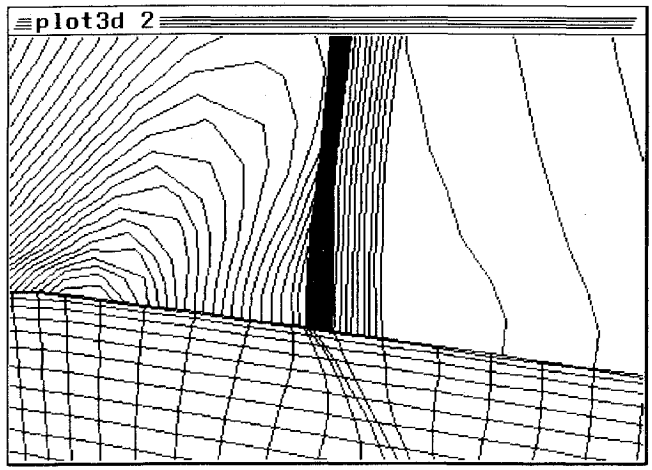

Fig. 6 Shock with adaptive grid.

Adaptive grids were generated at 200, 300, 400, 500, and 600 cycles of solution calculations. Then the solution calculations were carried out to 1000 cycles. It is clear from the fifth adaptive grid, shown in Fig. 3, that the grid lines are clustering around the areas where the shocks occur. Figure 4 shows that the grid lines cluster more closely on the leeward side of the body and then gradually relax the clustering effect in the circumferential direction toward the windward side, exactly in response to the characteristics of the shock there. Also notice that the slopes of grid lines are smooth across the boundaries between the shocks. It is clear from the pressure contours displayed in both Figs. 5 and 6 that the shock obtained with the adaptive grid is much more accurately defined than that without adaptations. The overall pressure distribution along the body, however, was slightly improved, and the extra central process time needed for five adaptations was about 3.4% over that of the nonadaptive approach in this test case. In summary, the solution-adaptive grid generation technique does provide proper composite-grid networks for simulations of aerodynamics around complex three-dimensional geometries.

References

[1]Kim, H. J., and Thompson, J. F., "Three-Dimensional Adaptive Grid Generation on a Composite Block Grid," AIAA Paper 88-0311, Jan. 1988.

[2]Thompson, J. F., Warzi, Z. U. A., and Mastin, C. W., *Numerical Grid Generation: Foundations and Applications,* North-Holland, Amsterdam, The Netherlands, 1985.

[3]Tu, Y., and Thompson, J. F., "Three-Dimensional Solution-Adaptive Grid Generation on Composite Configurations," AIAA Paper 90-0329, Jan. 1990.